Carcinogenesis vol.11 no.9 pp.1531–1538, 1990

Ultrastructural changes in chemically induced preneoplastic focal lesions in the rat liver: a stereological study

E.M.Jack, W.Stäubli, F.Waechter, P.Bentley, J.Suter, F.Bieri, S.F.Muakkassah-Kelly and L.M.Cruz-Orive[1]

Central Toxicology Unit, Ciba-Geigy Ltd, CH-4002 Basel and [1]Stereology Unit, Department of Anatomy, University of Bern, CH-3000 Bern, Switzerland

Ultrastructural changes were investigated and quantified, using a stereological approach, in early gamma-glutamyltranspeptidase (GGT)-positive focal lesions, induced in the rat liver by treatment with a single initiating dose of diethylnitrosamine (DENA) followed by promotion with phenobarbitone (PB) for 30 weeks. Within the extra-hepatocyte environment of focal tissue, the mean volume occupied by Ito cells was markedly decreased, whilst that occupied by endothelial and Kupffer cells was increased, when compared to uninvolved tissue from the same rat livers. The bile canaliculi were dilated, but no significant differences in the mean volume occupied by the sinusoidal and Disse spaces were noted. In focal hepatocytes there was a striking overproduction of lipid droplets and proliferation of smooth endoplasmic reticulum (sER). Whorls of concentrically arranged, parallel ER membranes were found only in the hepatocytes of preneoplastic foci, in association with the proliferated sER, and never in the surrounding, uninvolved tissue. The increase in mean volume of the sER, lipid droplet and cytoplasmic matrix compartments, together with the appearance of whorls, were the major contributing factors to the marked hypertrophy seen in focal hepatocytes. The mean volume of the rough endoplasmic reticulum, mitochondrial, lysosomal, peroxisomal and nuclear compartments per hepatocyte also increased, but contributed to a lesser extent to the cellular hypertrophy. It is speculated that whorls may be structural adaptations, resulting from a possible alteration in the normal feedback control of cholesterol synthesis, for the production of sterols and the biogenesis of sER in eosinophilic-type focal cells. The significance of changes observed in focal tissue, and the high biological variation noted between foci, is discussed in relation to the hepatocarcinogenic process.

Introduction

Experimentally induced hepatocarcinogenesis in rodents is generally regarded as a multistep process (see reviews 1–4). The first morphological indications of chemically induced carcinogenic change in the liver are the appearance of areas or foci of phenotypically altered cells. Neoplastic nodules and, subsequently, hepatocellular carcinomas develop at later stages in the chronological progression of hepatocarcinogenesis. Foci are, therefore, believed to represent preneoplastic stages and may, consequently, be important as early indicators of potential neoplastic change (5).

Foci of altered cells have been widely studied morphologically and histochemically for differences in enzyme activities using light microscopy (LM*) (reviewed in 4). In contrast, there have been few ultrastructural investigations of foci of altered cells (6–8), probably because of the difficulty in recognizing focal tissue using electron microscopy (EM). Hirota and Williams (7) studied foci by EM using iron as an electron-dense marker to distinguish iron-resistant lesions from the rest of the liver. No detailed ultrastructural investigation and quantification of alterations within preneoplastic foci, however, has been reported before.

In order to characterize early focal changes during hepatocarcinogenesis, we have adapted a stereological approach to investigate and quantify alterations within the extra-cellular, cellular and sub-cellular compartments of preneoplastic lesions. In addition to stereological ratios, absolute quantities were also estimated. The limitations of many stereological studies, which report only ratios when drawing conclusions about the functional significance of the biological changes, has often been stressed (9). Foci were chemically induced in the liver of rats using diethylnitrosamine (DENA) as an initiator and phenobarbitone (PB) as a promoter, according to the Peraino method (10). To our knowledge, no previous study has investigated the ultrastructure of early hepatocarcinogenic changes induced by these two compounds, which are used in several models of liver cancer (reviewed in 4). Focal lesions were identified by the presence of gamma-glutamyltranspeptidase (GGT) using LM and then selected for EM. GGT is known to mark 80–85% of all preneoplastic foci produced by the Peraino protocol (10).

PB as a promoter of liver growth after initiation with a genotoxic carcinogen, evokes a pleiotropic response characterized by an increase in cell proliferation and induction of drug-metabolizing enzymes (11). Changes in the ploidy levels and in the percentage of binucleated cells, in response to the mitogenic effect of PB in DENA-initiated focal lesions, have been recently reported (12). The effect of PB as a stimulator of cellular hypertrophy in the foci was also assessed, revealing a marked increase in mean hepatocyte volume (12). The sub-cellular changes underlying this hypertrophic response evoked by PB in focal hepatocytes are investigated in this present EM study using the same material.

Materials and methods

Treatment of animals

GGT-positive foci were induced in newborn female rats (Tif:RAIf strain) using DENA as the initiator and PB as the promoter following the protocol of Peraino *et al.* (10). DENA (Fluka AG, Buchs, Switzerland) was administered i.p. (15 mg/kg body wt in 0.9% NaCl) 24 h after birth. At the age of 3 weeks, the offspring were weaned and fed a casein-enriched (30%) diet, Nafag no. 900 (Nafag AG, Gossau, Switzerland), which contained 500 p.p.m. PB (Fluka) for 30 weeks. After fasting for 20 h, three animals were anaesthetized with Nembutal (Abbott AG, Zug, Switzerland) and were perfused with 0.9% NaCl and 0.1% heparin for 2 min, followed by perfusion with 3% paraformaldehyde and 0.4% glutaraldehyde in 0.1 M phosphate buffer (pH 7.4) for 10 min.

*Abbreviations: LM, light microscopy; EM, electron microscopy; rER, rough endoplasmic reticulum; DENA, diethylnitrosamine; PB, phenobarbitone; GGT, gamma-glutamyltranspeptidase; sER, smooth endoplasmic reticulum; TGFβ, transforming growth factor β; HMGCoAR, 3-hydroxy-methylglutaryl coenzyme A reductase.

© Oxford University Press

Stereological analysis

Objectives. As outlined in Figure 1, the following parameters were estimated for the various compartments in preneoplastic lesions and extra-focal tissue from the same rat livers: (i) the volume ratio (V_v), and the mean volume ($\bar{V}$), of the extracellular spaces and the sinusoidal cells per hepatocyte; (ii) the volume ratio, and the mean volume, of the organelle compartments per hepatocyte; (iii) the surface ratio (S_v), and the mean surface area ($\bar{S}$), of the hepatocyte plasma membrane domains per hepatocyte.

Tissue sampling and processing for stereology.

(i) Each liver lobe was cut into slices (~5 mm thick) which were then cut into strips (~3.5 mm wide).

(ii) Three strips were systematically chosen per liver and immersed in 3% paraformaldehyde and 0.4% glutaraldehyde in 0.1 M phosphate buffer for 1 h at 4°C and kept in 0.1 M phosphate buffer containing 5% saccharose at 4°C prior to vibratome sectioning.

(iii) Each strip was cut into a series of 100 μm thick vibratome sections (~5 × 3.5 × 0.1 mm^3).

(iv) Focal tissue was identified in each set of the vibratome sections by its positive staining for GGT (13). GGT-negative tissue was regarded as uninvolved, extra-focal tissue. Two sections were systematically chosen per set of vibratome sections.

(v) A block of GGT-positive focal tissue (0.5 × 0.5 × 0.1 mm^3) was trimmed out of one section, and a block of uninvolved tissue of the same size from the other section. Care was taken not to include surrounding, uninvolved tissue when trimming out the foci. For this reason, foci with an area >0.25 mm^2 were selected. In non-focal tissue, it was confirmed by LM examination of semi-thin sections, that cells from all lobular zones were included in each block sampled. A total of three blocks of foci and three blocks of extra-focal tissue per animal were selected in this way.

(vi) The blocks were post-fixed in 3% glutaraldehyde in 0.1 M cacodylate buffer, pH 7.4, for 3 h at 4°C, and then in 1% osmium tetroxide in the same buffer for 1 h at 4°C, dehydrated through a series of acetone solutions and embedded in Epon.

(vii) Ultra-thin (70 nm) sections were cut from the top and bottom of each block, using a Reichert 'ultracut' microtome, for ultrastructural stereological analysis. The sections were mounted on 200 mesh copper grids which were coated with a carbon-coated parlodion film, and stained with 5% uranyl acetate and Reynolds lead citrate. The remaining tissue in the block was used for LM to estimate the mean hepatocyte volume (12).

Selection of magnifications and fields. The stereological analysis was made at three different levels of magnification. Figure 1 shows the various compartments which were analysed for each block of focal tissue and extra-focal tissue per animal, and at which magnification this analysis was made.

One section from the top and from the bottom of the tissue block was examined per magnification level with a Philips transmission electron microscope (EM-300). Fifteen fields on each tissue section were systematically sub-sampled (14). The upper right corner of each of the 15 fields was photographed, at the primary magnifications of ×2000, ×6800 and ×33 000, onto 35 mm film. In this way, a total of 30 micrographs per magnification level were recorded per tissue block. Contact films were made from the 35 mm negatives and the micrographs were projected in a table projector unit, onto a glass screen displaying a test grid of 57 600 mm^2 in area. The final projected magnifications were ×6500, ×20 000 and ×97 000.

Analysis of micrographs. The volume ratio and surface ratio of the various compartments investigated in the preneoplastic lesions and the extra-focal tissue (Figure 1) were estimated by point counting methods (15). Micrographs at ×6500 were examined using a square lattice test system containing 144 points (with an area to test point ratio of 3.9 cm^2). Micrographs of ×20 000 were examined using a multipurpose test system containing 168 points and 84 lines of 20 mm in length [with an area to test point ratio of 3.4 cm^2, and a test point to test line length ratio (p/l) of 1 cm^{-1}]. Micrographs at ×97 000 were examined using a multipurpose test system containing 42 points and 21 lines of 40 mm in length (with an area to test point ratio of 13.5 cm^2, and a test point to test line length ratio of 0.5 cm^{-1}).

(i) *Volume ratio* (V_v, μm^0). The volume ratio (the ratio of the volume of a compartment to the volume of the reference space, $\mu m^3/\mu m^3$), also termed the volume fraction, was estimated for each compartment by dividing the sum of all points that fell on that compartment by the sum of all the points that fell on the reference space. For example, for a given block, the ratio of mitochondrial volume to hepatocyte volume was estimated as follows:

$$\text{est } V_v \text{ (mito, hepatocyte)} = \sum_{i=1}^{n} P_i \text{ (mito)} / \sum_{i=1}^{n} P_i \text{ (hepatocyte)}$$

where $\Sigma_{i=1}^{n} P_i$ denotes the sum of point counts over n micrographs from the same block. For the extracellular spaces and sinusoidal spaces, evaluated at ×6000, the reference space was the hepatocyte although this was not the containing space. The reference space for the organelles evaluated at ×20 000 was the hepatocyte, and at ×97 000 the hepatocyte cytoplasm. To convert the volume ratios of the organelles per cytoplasm (evaluated at ×97 000) to volume ratios per hepatocyte, the ratios were multiplied by the ratio of cytoplasm volume to hepatocyte volume (estimated at ×20 000). For example:

$$\text{est } V_v \text{ (sER/cell)} = V_v \text{ (sER/cytoplasm)} \times V_v \text{ (cytoplasm/cell)}$$

The volume ratios are expressed as a percentage in Tables I and II.

(ii) *Surface ratio* (S_v, μm^{-1}). The surface ratio (the ratio of the surface area of a compartment to the volume of the reference space, $\mu m^2/\mu m^3$) was estimated by counting the number of intersection points (I) between the membranes and the test lines, and the number of test points (P) which hit the reference space, according to the classical stereological formula $S_v = 2I_L$ (15) which, in practical terms, reads:

$$\text{est } S_v = 2\, p/l \, \frac{\sum_{i=1}^{n} I_i}{\sum_{i=1}^{n} P_i}$$

where p/l is the ratio of test points to test line length (real units) and $\Sigma_{i=1}^{n} I_i$

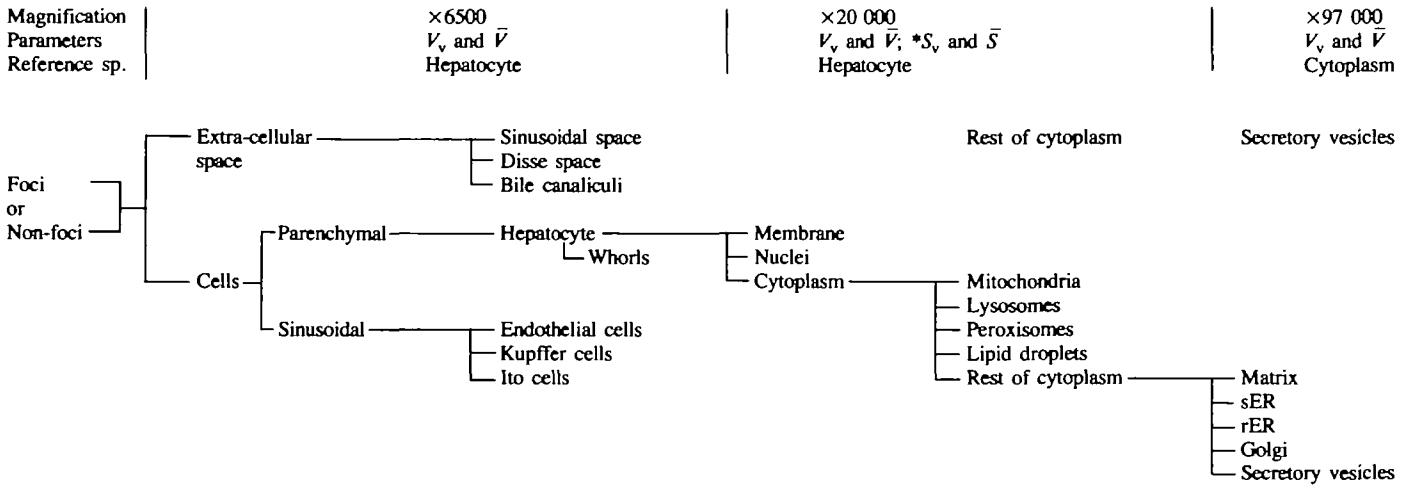

Fig. 1. Multilevel sampling of compartments, in preneoplastic foci and extra-focal (non-foci) areas from the same liver, for stereological analysis at the EM level. The volume ratio (V_v, μm^0) and the mean surface ratio (S_v, μm^{-1}) were estimated by point counting methods. The mean volume ($\bar{V}$) and the mean surface area ($\bar{S}$) of each compartment per hepatocyte were calculated by multiplying the volume ratio and surface ratio respectively by the mean hepatocyte volume (the reference space volume) which was estimated independently in a parallel study (12).

and $\Sigma_{i=1}^{n} P_i$ are the total intersection counts and total point counts respectively, in the n micrographs of the block examined.

(iii) *Mean volume* ($\bar{V}$) *and mean surface area* ($\bar{S}$). Absolute values of the volumes and surface areas per hepatocyte were calculated by multiplying the respective volume and surface ratios [estimated as indicated in (i) and (ii) above] by the mean hepatocyte volume $\bar{V}$(hep) (the reference space volume), for example:

$$\text{est } \bar{V}(\text{sER}),\ \mu\text{m}^3 \text{ per hepatocyte} = \text{est } \bar{V}(\text{hep})\ \mu\text{m}^3 \times \text{est } V_v(\text{sER/hep})$$

The mean hepatocyte volume was estimated at the LM level using hepatocytes sampled from semi-thick sections which were taken from the same tissue blocks as the ultra-thin sections (12).

Statistical analysis

The biological variation between blocks of focal tissue, and between blocks of non-focal tissue, was derived by subtracting the mean variance within blocks (the stereological error variance) from the total variance between blocks of the volume or surface area estimate (16). Group means within foci and non-foci were compared using a two-tailed Wilcoxon's two-sample rank test (17) with three matched sets (corresponding to the three animals) and three scores for each of the two groups (namely, three blocks of foci and three of non-foci) within each animal. A P-value of <0.05 was considered statistically significant.

Results

Foci of phenotypically altered cells were induced by treating rats with PB for 30 weeks after a single dose of DENA. Uninvolved, extra-focal tissue (Figure 2) was compared to focal tissue (Figure 3), identified by the presence of the enzyme GGT, to investigate alterations specific to the early preneoplastic state. Due to proliferation of the smooth endoplasmic reticulum (sER), all the foci studied were eosinophilic in nature; no clear cell foci, which are characterized by glycogen storage, were seen. No tumours were observed at this stage in the hepatocarcinogenic process.

For many of the compartments studied, a decrease in the volume ratio or surface ratio, but an increase in the mean volume or surface area, was noted in focal tissue (Tables I–III). This was due to the striking increase in the mean hepatocyte volume (the reference space volume) in focal tissue.

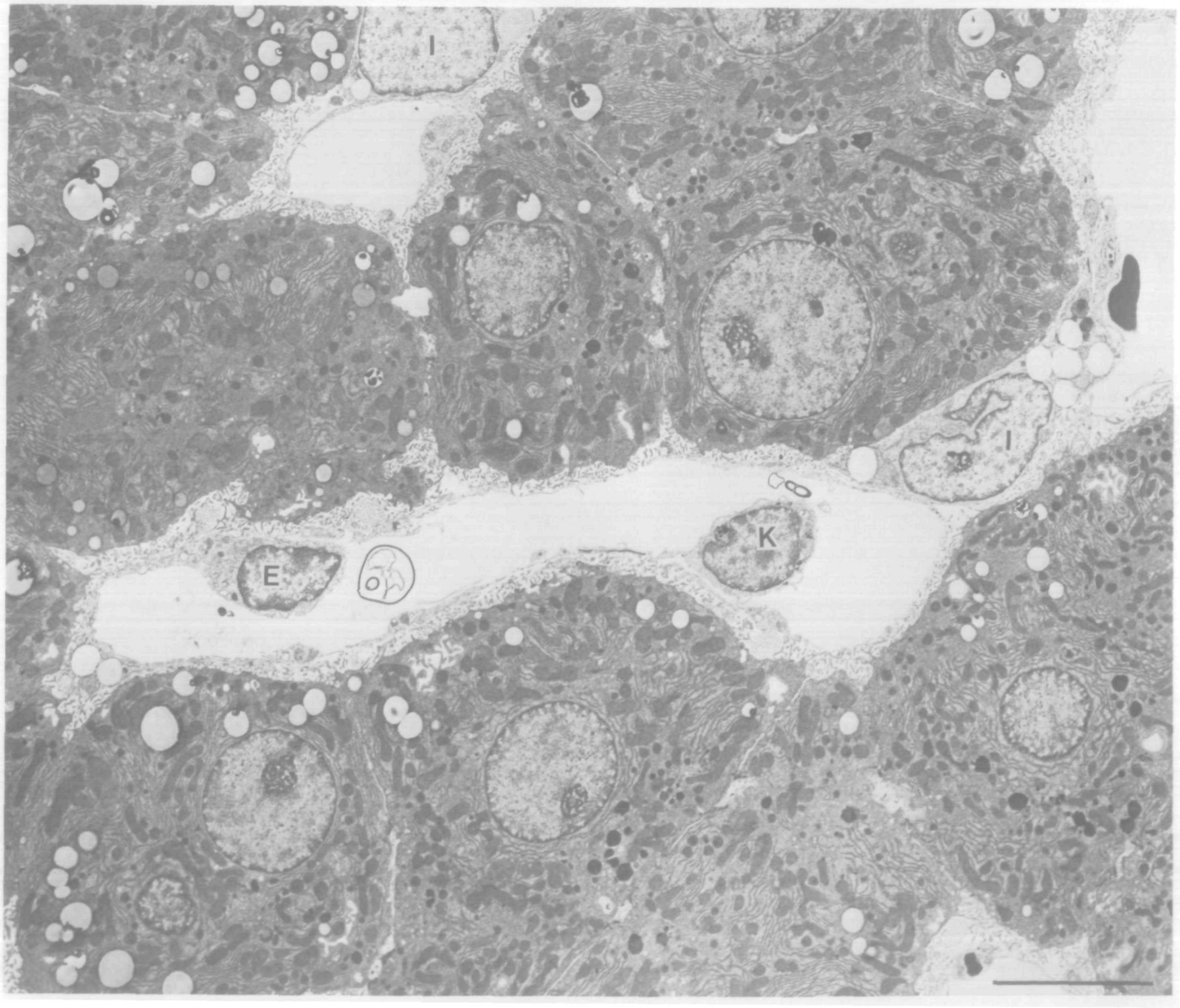

Fig. 2. Extra-focal, uninvolved liver from a rat treated for 30 weeks with PB after a single dose of DENA. The Ito cells (I) within the Disse space, the endothelial cells (E) lining the sinusoids and the Kupffer cells (K) in the sinsuoidal space constitute the non-hepatocyte, sinusoidal cell population of the liver. Bar = 8 μm.

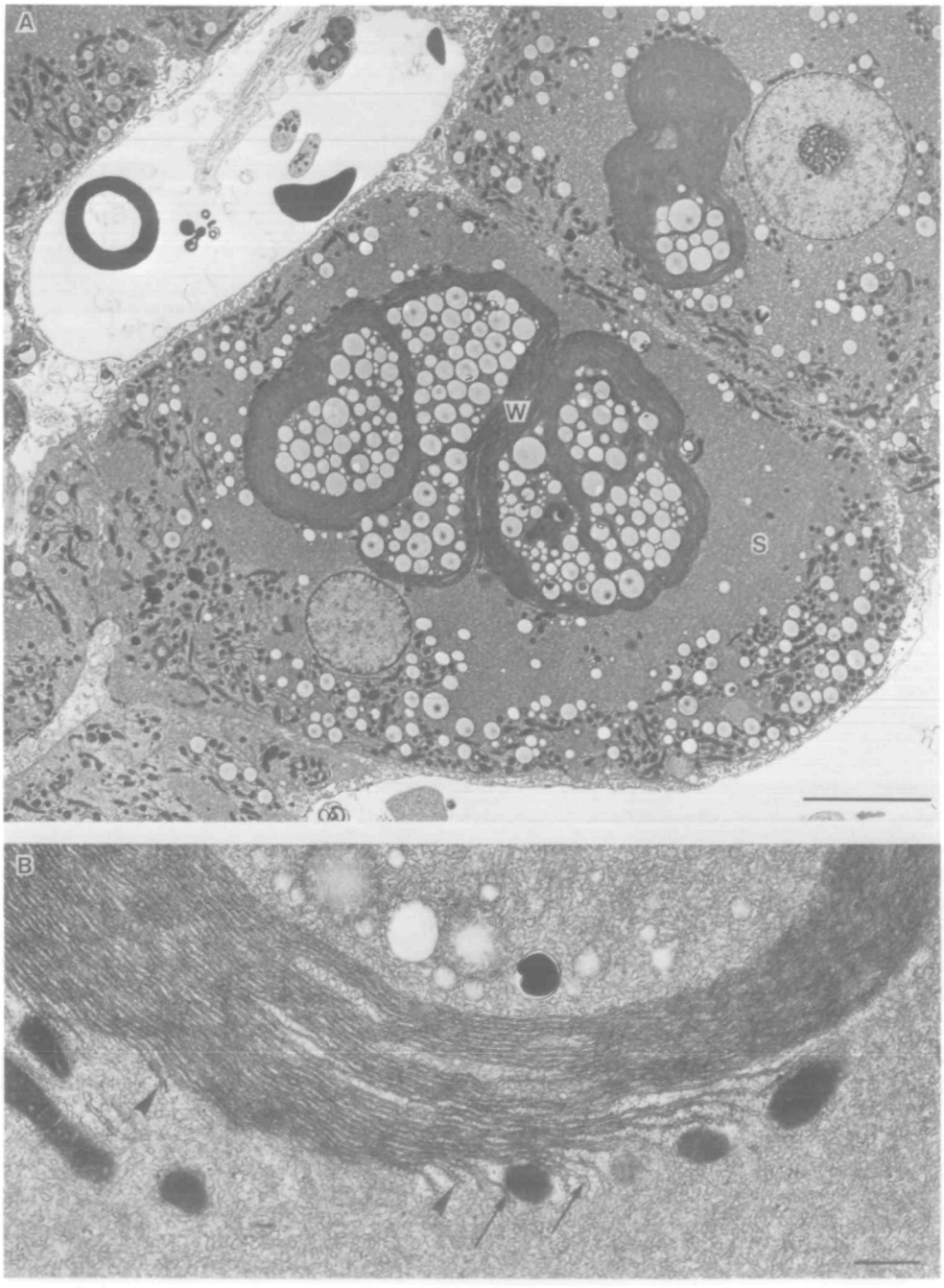

Fig. 3. GGT-positive, eosinophilic focal tissue from a rat treated for 30 weeks with PB after a single dose of DENA. (A) Note the increase in hepatocyte volume compared to non-focal tissue from the same rat liver (Figure 2), the proliferated sER (S) and the presence of whorl-like structures (W) containing lipid droplets and sER, which displace the rest of the organelles to the edge of the cell. (B) Parallel, closely packed ER membranes resembling rER are continuous with the proliferated sER inside and outside (arrows) the whorls, often via a short length of rER (arrowheads). Bar in (A) = 8 μm; in (B) = 0.5 μm.

Changes in extracellular space and sinusoidal cells (Tables I and II)

Many focal hepatocytes lost the polyhedral shape characteristic of cells from normal liver and non-focal tissue. Frequent widening of the intercellular space was noted between focal hepatocytes.

A decrease in the ratios of the volume of the sinusoidal space, Disse space and the sinusoidal cells (the endothelial, Kupffer and Ito cells) to the volume of the hepatocyte was noted in focal tissue (Table I). The mean volumes of the sinusoidal and Disse spaces per hepatocyte in focal tissue did not, however, differ significantly from that of non-focal tissue. The mean volumes occupied by endothelial and Kupffer cells were greater in focal tissue. In contrast, the mean volume occupied by the Ito cells decreased. In focal tissue, both the ratio of bile canalicular volume to hepatocyte volume, and the mean volume of the bile canaliculi per hepatocyte, increased.

The mean surface area of the sinusoidal, intercellular and bile canalicular plasma membrane domains per hepatocyte increased in focal tissue (Table II). There were, however, no significant differences in the proportions of the three membrane domains between focal and non-focal tissue. A loss of microvilli at the bile canalicular surface was noted in focal lesions.

Changes in hepatocyte organelles (Table III)

In all the foci studied there was a striking increase in the volume fraction and mean volume of sER and lipid droplets per

Table I. Summary of the stereological analysis of extracellular spaces and sinusoidal cells in GGT-positive focal lesions and extra-focal tissue from the same rat livers

Extracellular spaces and sinusoidal cells	Volume ratio, V_v		Volume (μm^3), $\bar{V}$ per hepatocyte		
	Non-foci (%)	Foci (%)	Non-foci	Foci	*P*
Sinusoidal space	18.9	9.1	1010 (42%)	1330 (48%)	NS
Disse space	8.3	4.3	450 (15%)	600 (33%)	NS
Bile canalicular space	0.5	0.8	30 (0%)	130 (36%)	***
Endothelial cells	3.6	2.4	190 (0%)	330 (22%)	***
Kupffer cells	1.0	0.8	50 (19%)	110 (0%)	**
Ito cells	1.3	0.2	70 (0%)	30 (0%)	**

Values are the means of nine tissue blocks from three animals. The volume ratio is expressed as a percentage. The biological variation between blocks, with the stereological variation removed, is indicated in parentheses.
Differences between focal and non-focal tissue were evaluated by means of a two-sample Wilcoxon's rank test (17), with the three animals regarded as three independent replications: NS, non-significant; $*P < 0.05$; $**P < 0.025$; $***P < 0.005$.

Table II. Summary of the stereological analysis of the plasma membrane domains in GGT-positive focal hepatocytes and non-focal hepatocytes from the same rat livers

Plasma membrane domains	Surface ratio, S_v (μm^{-1})		Surface area, $\bar{S}$ per hepatocyte (μm^2)			% of total plasma membrane		
	Non-foci	Foci	Non-foci	Foci	*P*	Non-foci	Foci	*P*
Sinusoidal	38	30	1990 (0%)[a]	4190 (0%)[a]	***	55 (11)[b]	59 (9)[b]	NS
Bile canalicular	14	9	750 (25%)	1170 (33%)	*	21 (7)	18 (9)	NS
Intercellular	16	12	840 (12%)	1680 (47%)	***	24 (7)	23 (6)	NS
Total plasma membrane	68	51	3580 (0%)	7040 (20%)		100	100	

Values are the means of nine tissue blocks from three animals.
[a]The biological variation between blocks with the stereological variation removed.
[b]The standard deviation.
Differences between focal and non-focal tissue were evaluated by means of a two-sample Wilcoxon's rank test (17), with the three animals regarded as three independent replications: NS, not significant; $*P < 0.05$; $**P < 0.025$; $***P < 0.005$.

Table III. Summary of the stereological analysis of hepatocyte organelles in GGT-positive focal lesions and extra-focal tissue from the same rat livers

Hepatocyte organelles	Volume ratio, V_v		Volume (μm^3), $\bar{V}$ per hepatocyte		
	Non-foci (%)	Foci (%)	Non-foci	Foci	*P*
sER	14.5	22.2	800 (39%)	3270 (51%)	***
Whorls:	–	4.9	–	690 (76%)	***
-ER membranes	–	3.2	–	440	
-lipid within	–	1.2	–	170	
-sER/matrix within	–	0.5	–	80	
Lipid droplets	3.0	7.3	160 (23%)	1290 (108%)	***
rER	6.4	4.8	340 (16%)	650 (18%)	***
Mitochondria	22.9	11.8	1220 (0%)	1670 (37%)	*
Lysosomes	1.4	0.8	80 (23%)	120 (35%)	*
Peroxisomes	1.5	1.0	80 (12%)	140 (36%)	***
Golgi	0.6	0.4	30 (0%)	40 (87%)	NS
Secretory vesicles	1.2	0.9	60 (0%)	120 (55%)	NS
Nucleus	8.1	4.9	430 (26%)	660 (0%)	**
Cytoplasmic matrix	40.4	41	2160 (11%)	6120 (56%)	***
Total hepatocyte	100	100	5360	14 770	

Values are the means of nine tissue blocks from three animals. The volume ratio is expressed as a percentage. The biological variation between blocks, with the stereological variation removed, is indicated in parentheses.
Differences between focal and non-focal tissue were evaluated by means of a two-sample Wilcoxon's rank test (17), with the three animals regarded as three independent replications: NS, non-significant; $*P < 0.05$; $**P < 0.025$; $***P < 0.005$.

hepatocyte. In addition, whorl-like structures, found in association with the proliferated sER, were observed (Table III; Figures 3 and 4). The volume fraction of the other organelles in focal hepatocytes decreased, although their mean volume slightly increased. For all the compartments except the nucleus, the biological variation was greater between blocks of focal tissue than between non-focal tissue. This was particularly marked in the sER, lipid droplets and whorl compartments.

Whorl-like structures were found in all foci but never in the extra-focal tissue (Figure 4). They were located in fields of proliferated sER which displaced the other hepatocyte organelles to the cell perimeter. The whorls appeared to be approximately oval or cylindrical in shape and were made up of tightly packed, concentric ER membranes which resembled rough endoplasmic reticulum (rER) and enclosed a lumen containing lipid droplets and sER tubules (Figure 3). The parallel whorled ER membranes

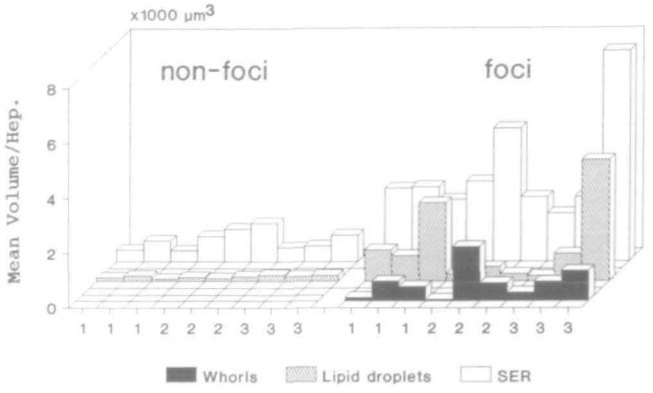

Fig. 4. Changes in the mean volume of sER, lipid droplets and whorls per hepatocyte (Hep.) from nine GGT-positive focal lesions compared to nine blocks of non-focal tissue from the same rat livers. 1, 2 and 3 denote tissue blocks from animals 1, 2 and 3 respectively.

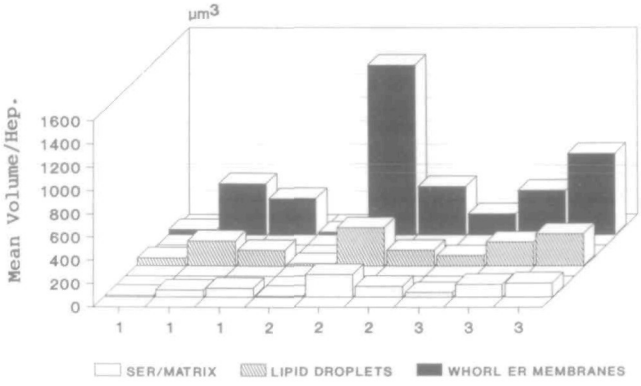

Fig. 5. Comparison of the mean volume of whorl components per hepatocyte (Hep.) from nine different GGT-positive, eosinophilic focal lesions. The parallel, whorled ER membranes enclose a space containing lipid droplets, sER and cytoplasmic matrix. 1, 2 and 3 denote foci from animals 1, 2 and 3 respectively.

were continuous with the rER, and with the proliferated sER both within the whorls and outside the whorls (Figure 3B). Short stretches of rER appeared often to link the parallel ER membranes with the sER membranes. Figure 5 shows the relationship between the mean volume of whorled membranes, the lipid droplets, and the sER and matrix within the whorls per hepatocyte (Figure 5). A close correlation ($r = 0.9$) was noted between the whorled membranes and the lipid droplets.

In uninvolved hepatocytes, the rER was arranged in normal parallel stacks. In focal hepatocytes, however, the rER cisternae were dispersed and of varying lengths—features that appear to be associated with the development of liver neoplasia (18).

The mean hepatocyte volume in focal tissue increased by almost 3-fold (12). The contribution of each sub-cellular compartment to this hypertrophic response is illustrated in Figure 6, by expressing the increase in the mean volume of each organelle per hepatocyte as a percentage of the increase in mean hepatocyte volume.

Discussion

Methodological considerations

The importance of estimating the reference space volume in a stereological analysis, in order to express parameters not only as ratios but also in absolute terms, has been often stressed (see

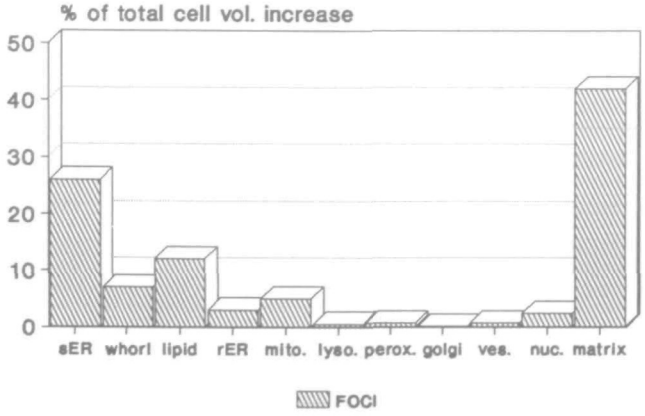

Fig. 6. The contribution of each sub-cellular compartment to the increase in hepatocyte volume (hypertrophy) in preneoplastic focal lesions. The increase in the mean volume of each hepatocyte compartment is expressed as a percentage of the increase in mean cell volume.

ref. 9 for comments about the 'Reference trap') and is illustrated in this present study. The reference space volume may change under different experimental conditions, making the interpretation of ratios alone difficult. This has important implications when the functional consequences of changes in compartments are being discussed. A decrease in the volume or surface ratio of a compartment does not necessarily imply that the volume or surface area of that compartment has actually decreased.

In the present study, the hepatocyte was defined as the reference space for the stereological analysis of changes in hepatocyte organelles in GGT-positive focal tissue compared to non-focal tissue. The hepatocyte was also used as the reference space for the analysis of changes in the extracellular spaces and sinusoidal cells. There are strong indications that preneoplastic foci represent clonal expansions of single initiated cells (reviewed in 19). It was, therefore, considered appropriate to express the volumes of extracellular spaces and the sinusoidal cells per volume of uninvolved hepatocytes (in non-focal tissue) or per volume of focal hepatocytes (in preneoplastic lesions). The mean hepatocyte volume was estimated independently from the same tissue blocks in a parallel study (12). Absolute quantities could, therefore, be calculated by multiplying the stereological ratios by the mean hepatocyte volume. Thus a true increase or decrease in the mean volume or mean surface area of the compartments could be determined.

Changes in the extra-hepatocyte environment in focal lesions

In preneoplastic foci the bile canalicular lumina were dilated with a loss of microvilli. These features resembled the pathological condition of cholestasis in which the excretion of bile is impaired (20) and have also been described in hepatic neoplastic nodules and tumours (8,21,22). The volume occupied by the sinusoidal and the Disse spaces in focal tissue did not differ significantly from that of non-focal tissue.

Cell-to-cell contact appeared to be reduced between focal hepatocytes as indicated by a frequent widening of the intercellular space. It has been speculated that a reduced intercellular contact in focal lesions could inhibit the intercellular transfer of normal growth factors and differentiation factors which are required to maintain homeostasis and would, therefore, favour the persistence of focal cells and their progression to the neoplastic state (23).

A decrease in the volume occupied by the Ito cells (also termed fat-storing, lipocytes or stellate cells) was noted in focal lesions.

This is of interest with regard to a recent report that transforming growth factor β (TGFβ), an inhibitor of hepatocyte DNA synthesis, was found in the sinusoidal cell population. Fausto and Mead (24) have suggested that TGFβ functions as a paracrine inhibitor of hepatocyte DNA synthesis to prevent uncontrolled proliferation during liver regeneration. In this context, it could be speculated that a reduction in Ito cells may be involved in the loss of the normal regulation of cell proliferation in focal tissue. Ito cells are known to be the major hepatic storage site of vitamin A (reviewed in 25). Consequently, the observed change in Ito cells may reflect an altered storage of vitamin A in focal lesions.

The mean volume occupied by the endothelial and Kupffer cells was slightly larger than that found in non-focal tissue. When compared to untreated rat liver (26), the volume occupied by Kupffer cells (the resident macrophage population), in both focal and non-focal tissue, appeared to be reduced. This supports the results of a previous study in which a progressive decrease in the percentage of Kupffer cells during the hepatocarcinogenic process was reported (27). Kupffer cells are involved in many normal hepatic functions (28). A decrease in these functions, through a reduction in the percentage of Kupffer cells, may be of importance in the development of focal lesions.

Sub-cellular changes in focal hepatocytes

The most striking changes in DENA-initiated focal hepatocytes were the formation of whorl-like structures and an overproduction of sER and lipid droplets. In contrast to the focal hepatocytes, no whorls were ever observed in uninvolved, non-focal hepatocytes. Interestingly, the amount of sER proliferation in non-focal hepatocytes after 30 weeks treatment with PB (following a single dose of DENA) was very similar to that reported after short-term treatment with PB alone (29).

The proliferation of sER, production of lipid droplets and appearance of whorls, together with the expansion of the cytoplasmic matrix, were the major contributing factors to the almost 3-fold increase in the mean focal hepatocyte volume which was estimated in a parallel study in focal tissue (12). The mean volumes occupied by the rER, mitochondrial, lysosomal, peroxisomal and nuclear compartments also increased significantly per focal hepatocyte, but contributed to a lesser extent to the cellular hypertrophy.

Extensive proliferation of sER has been noted in other studies of preneoplastic and neoplastic stages of liver cancer (6–8,22,30) and appears to be characteristic of eosinophilic cell types. The proliferation of sER in GGT-positive preneoplastic lesions, which is accompanied by increased levels of PB-inducible P450 isoenzymes (31), could be associated with an increased production of active oxygen through modulation of the cytochrome P450 electron transport chain. The production of oxygen radicals has been reported in liver microsomal preparations from PB-treated rats (32). There is evidence that an increased concentration of active oxygen can promote initiated cells to neoplastic growth (33).

In this present study, the whorl-like structures were always found in association with proliferated sER. They were made up of whorled, parallel arrays of ER membranes that resembled rER and enclosed a lumen containing accumulations of lipid droplets. Their membranes were often continuous with the rER. It is possible that they originate from rER and are packed into whorled arrays by spiral coiling along the length of the structure, giving rise to sER intermittently within the whorl and to the proliferated sER lakes at the opposite end of the whorl. Due to their close association with proliferated sER, whorls could be regarded as structural adaptations in focal cells providing a high density of membranes to accommodate the enzymes and other membrane components involved in the synthesis of sER.

Whorl-like structures (fingerprints or concentric lamellar arrays), have been described in association with proliferated sER (i) in normal steroid secreting tissue such as the adrenal cortex (34) and the testes (35); (ii) in the liver of rats treated subchronically with various hepatotrophic agents (reviewed in 36) and in hepatocyte cultures treated with nafenopin, a liver tumour promoter (37); and (iii) in preneoplastic lesions (6), neoplastic nodules and/or liver tumours after treatment with various carcinogens including DENA (38), DENA/2-acetylaminofluorene (8,21), PB (30) and aflatoxin (22).

Recently, whorls were demonstrated to be reversibly induced in the liver of rats during short-term treatment with inhibitors of 3-hydroxy-methylglutaryl coenzyme A reductase (HMGCoAR). These whorls were shown to be rich in HMGCoAR (39,40). This enzyme catalyses the rate-limiting step in cholesterol biosynthesis and, in normal liver, is subject to multivalent negative feedback suppression by sterols and non-sterol derivatives (41). HMGCoAR is normally located in the sER and rER (42). In the light of these recent studies using HMGCoAR inhibitors, and the occurrence of whorls in normal tissue that is specialized in steroid production, it is interesting to speculate that the formation of whorls in the liver could be associated with an altered cholesterol synthesis. Increased cholesterol synthesis has been reported in the liver of rats treated with the hepatocarcinogens DENA and PB (43). Furthermore, the loss of normal feedback inhibition of cholesterol synthesis has been well characterized in malignant and premalignant hepatic tissue (44).

We would, therefore, suggest that whorls in preneoplastic foci could also contain high levels of HMGCoAR, resulting from an alteration in the normal feedback inhibition of cholesterol on HMGCoAR in focal cells. It is possible that whorls may be sites of elevated HMGCoAR activity for the increased production of cholesterol, which may, in turn, be involved in the biosynthesis of sER. The accumulation of lipid droplets within the whorl lumen could indicate a saturation of cholesterol levels within the cell, since lipid droplets are known to store cholesterol and/or its esters (45).

The high biological variation between foci, particularly in lipid droplet content, possibly reflects focal cell populations at different stages in development during the course of hepatocarcinogenesis. Vacuolated (fat-storing) cells, together with clear, eosinophilic and basophilic cell types, have been described in mixed-cell type foci which appear at a later stage in liver carcinogenesis than eosinophilic foci (6). A sequential phenotypic conversion of altered cells, from early appearing clear and eosinophilic foci through intermediate, mixed cell and basophilic foci, to neoplastic nodules and, ultimately, carcinomas, during the hepatocarcinogenic process has been proposed (reviewed in 1). Clear and eosinophilic foci show only a slightly increased cell proliferation, whilst the appearance of mixed and basophilic cell populations in foci, nodules and carcinomas is associated with a pronounced and steadily increasing cell proliferation (1). In view of this concept of sequential cellular alteration, the storage of lipid droplets and the accumulation of sER membranes observed in this present study may be regarded as adaptive steps in preparation for subsequent changes to a more rapidly dividing and organelle-poor basophilic cell type.

Acknowledgements

The expert technical assistance of C.Zimmermann and K.Brändli, and photographic assistance of I.Förster is gratefully acknowledged. L.M.C.O. acknowledges support from the SNSF, grant no. 31-8838.86.

References

1. Bannasch,P., Enzmann,H., Hacker,H.J., Weber,E. and Zerban,H. (1989) Comparative pathobiology of hepatic preneoplasia. In Bannasch,P., Keppler,D. and Weber,G. (eds), *Falk Symposium 51. Liver Cell Carcinoma*. Kluwer, Dordrecht, pp. 55–76.
2. Farber,E. and Sarma,D.S.R. (1987) Hepatocarcinogenesis: a dynamic cellular perspective. *Lab. Invest.*, **56**, 4–22.
3. Moore,M.A. and Kitagawa,T. (1986) Hepatocarcinogenesis in the rat: the effect of promoters and carcinogens *in vivo* and *in vitro*. *Int. Rev. Cytol.*, **101**, 125–173.
4. Peraino,C., Richards,W.L. and Stevens,F.J. (1983) Multistage hepatocarcinogenesis. In Slaga,T.J. (ed.), *Mechanisms of Tumor Promotion*. CRC Press, Boca Raton, FL, Vol. 1, pp. 1–53.
5. Bannasch,P. (1986) Preneoplastic lesions as end points in carcinogenicity testing. I. Hepatic preneoplasia. *Carcinogenesis*, **7**, 689–695.
6. Bannasch,P., Mayer,D. and Hacker,H.J. (1980) Hepatocellular glycogenosis and hepatocarcinogenesis. *Biochim. Biophys. Acta*, **605**, 217–245.
7. Hirota,N. and Williams,G.M. (1982) Ultrastructural abnormalities in carcinogen-induced hepatocellular altered foci identified by resistance to iron accumulation. *Cancer Res.*, **42**, 2298–2309.
8. Ogawa,K., Medline,A. and Farber,E. (1979) Sequential analysis of hepatic carcinogenesis. A comparative study of the ultrastructure of preneoplastic, malignant, prenatal, postnatal, and regenerating liver. *Lab. Invest.*, **41**, 22–35.
9. Braendgaard,H. and Gundersen,H.J.G. (1986) The impact of recent stereological advances on quantitative studies of the nervous system. *J. Neurosci. Methods*, **18**, 39–78.
10. Peraino,C., Carnes,B.A., Stevens,F.J., Staffeldt,E.F., Russell,J.J., Prapuolenis,A., Blomquist,J.A., Vesselinovitch,S.D. and Maronpot,R.R. (1988) Comparative developmental and phenotypic properties of altered hepatocyte foci and hepatic tumors in rats. *Cancer Res.*, **48**, 4171–4178.
11. Schulte-Hermann,R. (1987) Initiation and promotion in hepatocarcinogenesis. *Arch. Toxicol.*, **60**, 179–181.
12. Jack,E.M., Bentley,P., Bieri,F., Muakkassah-Kelly,S., Stäubli,W., Suter,J., Waechter,F. and Cruz-Orive,L.M. (1990) Increase in hepatocyte volume and nuclear volume, and decrease in the population of binucleated cells, in preneoplastic foci of rat liver: a stereological study using the nucleator method. *Hepatology*, **11**, 286–297.
13. Rutenburg,A.M., Kim,H., Fischbein,J., Wasserkrug,H.C. and Seligman,R. (1969) Histochemical and ultrastructural demonstration of gamma-glutamyl transpeptidase activity. *J. Histochem. Cytochem.*, **17**, 517–526.
14. Müller,A.E,. Cruz-Orive,L.M., Gehr,P. and Weibel,E.R. (1981) Comparison of two subsampling methods for electron microscopic morphometry. *J. Microsc.*, **123**, 35–49.
15. Weibel,E.R. (1979) *Stereological Methods, Vol. 1: Practical Methods for Biological Morphometry*. Academic Press, London.
16. Gundersen,H.J.G .and Osterby,R. (1981) Optimizing sampling efficiency of stereological studies in biology: or 'Do more less well!' *J. Microsc.*, **121**, 65–73.
17. Meddis,R. (1984) *Statistics Using Ranks: A Unified Approach*. Basil Blackwell, Oxford.
18. Winton,D.J., Flaks,B. and Flaks,A. (1988) Quantitative electron microscopy of carcinogen-induced alterations in hepatocyte rough endoplasmic reticulum. I. Chronic effect of 3'MeDAB and short-term effects of azo dyes of different carcinogenic potentials. *Carcinogenesis*, **9**, 987–999.
19. Rabes,H.M. (1989) Cell proliferation and clonal development in hepatocarcinogenesis. In Bannasch,P., Keppler,D. and Weber,G. (eds), *Falk Symposium 51. Liver Cell Carcinoma*. Kluwer, Dordrecht, pp. 305–313.
20. Phillips,M.J., Poucell,S. and Oda,M. (1986) Mechanisms of cholestasis. *Lab. Invest.*, **54**, 593–608.
21. Heijden van der,C.A. and Dormans,J.A.M.A. (1981) Short-term induction of neoplastic nodules in the rat liver. II. Study of their development and the effects of withdrawal of 2-acetylaminofluorene. *Carcinogenesis*, **2**, 147–156.
22. Pritchard,D.J. and Butler,W.H. (1988) The ultrastructural features of aflatoxin B_1-induced lesions in the rat liver. *Br. J. Exp. Pathol.*, **69**, 793–804.
23. Williams,G.M. (1981) Liver carcinogenesis: the role for some chemicals of an epigenetic mechanism of liver tumour promotion involving modification of the cell membrane. *Food Cosmet. Toxicol.*, **19**, 577–583.
24. Fausto,N. and Mead,J.E. (1989) Regulation of liver growth: protooncogenes and transforming growth factors. *Lab. Invest.*, **60**, 4–13.
25. Fahimi,H.D. (1982) Sinusoidal endothelial cells and perisinusoidal fat-storing cells: structure and function. In Arias,I.M., Popper,H., Schachter,D. and Shafritz,D.A. (eds), *The Liver: Biology and Pathobiology*. Raven Press, New York, pp. 495–506.
26. Blouin,A., Bolender,R.P. and Weibel,E.R. (1977) Distribution of organelles and membranes between hepatocytes and non-hepatocytes in the rat liver parenchyma: a stereological study. *J. Cell Biol.*, **72**, 441–455.
27. Janossy,L , Zalatnai,A. and Lapis,K. (1986) Quantitative light microscopic study on the distribution of Kupffer cells during chemical hepatocarcinogenesis in the rat. *Carcinogenesis*, **7**, 1365–1369.
28. Jones,E.A. and Summerfield,J.A. (1988) Kupffer cells. In Arias,I.M., Jakoby,W.B., Popper,H., Schachter,D. and Shafritz,D.A. (eds), *The Liver: Biology and Pathobiology*. Raven Press, New York, pp. 683–704.
29. Stäubli,W., Hess,R. and Weibel,E. (1969) Correlated morphometric and biochemical studies on the liver cell. II. Effects of phenobarbital on rat hepatocytes. *J. Cell Biol.*, **42**, 92–112.
30. Feldman,D., Swarm,R.L. and Becker,J. (1981) Ultrastructural study of rat liver and liver neoplasms after long-term treatment with phenobarbital. *Cancer Res.*, **41**, 2151–2162.
31. Buchmann,A., Schwarz,M., Schmitt,R., Wolf,R., Oesch,F. and Kunz,W. (1987) Development of cytochrome P-450-altered preneoplastic and neoplastic lesions during nitrosamine-induced hepatocarcinogenesis in the rat. *Cancer Res.*, **47**, 2911–2918.
32. Kuthan,H. and Ullrich,V. (1982) Oxidase and oxygenase function of the microsomal cytochrome P450 monooxygenase system. *Eur. J. Biochem.*, **126**, 583–588.
33. Cerutti,P.A. (1985) Prooxidant states and tumor promotion. *Science*, **227**, 375–381.
34. Black,V.H. (1972) The development of smooth-surfaced endoplasmic reticulum in adrenal cortical cells of fetal guinea pigs. *Am. J. Anat.*, **135**, 381–417.
35. Christensen,A.K. (1965) The fine structure of testicular interstitial cells in guinea pigs. *J. Cell Biol.*, **26**, 911–935.
36. Stenger,R.J. (1970) Organelle pathology of the liver. The endoplasmic reticulum. *Gastroenterology*, **58**, 554–574.
37. Muakkassah-Kelly,S.F., Bieri,F., Waechter,F., Bentley,P. and Stäubli,W. (1988) The use of primary cultures of adult rat hepatocytes to study induction of enzymes and DNA synthesis: effect of nafenopin and electroporation. *Experientia*, **44**, 823–827.
38. Svoboda,D. and Higginson,J. (1968) A comparison of ultrastructural changes in rat liver due to chemical carcinogens. *Cancer Res.*, **28**, 1703–1733.
39. Li,A.C., Tanaka,R.D., Callaway,K., Fogelman,A.M. and Edwards,P.A. (1988) Localizaton of 3-hydroxy-3-methylglutaryl CoA reductase and 3-hydroxy-3-methylglutaryl CoA synthase in the rat liver and intestine is affected by cholestyramine and mevinolin. *J. Lipid Res.*, **29**, 781–796.
40. Singer,I.I., Scott,S., Kazazis,D.M. and Huff,J.W. (1988) Lovastatin, an inhibitor of cholesterol synthesis, induces hydroxymethylglutaryl-coenzyme A reductase directly on membranes of expanded smooth endoplasmic reticulum in rat hepatocytes. *Proc. Natl. Acad. Sci. USA*, **85**, 5264–5268.
41. Nakanishi,M., Goldstein,J.L. and Brown,M.S. (1988) Multivalent control of 3-hydroxy-3-methylglutaryl coenzyme A reductase. Mevalonate-derived product inhibits translation of mRNA and accelerates degradation of enzyme. *J. Biol. Chem.*, **263**, 8929–8937.
42. Reinhart,M.P., Billheimer,J.T., Faust,J.R. and Gaylor,J.L. (1987) Subcellular localization of the enzymes of cholesterol biosynthesis and metabolism in rat liver. *J. Biol. Chem.*, **262**, 9649–9655.
43. Gregg,R.G., Davidson,M. and Wilce,P.A. (1986) Cholesterol synthesis and HMG CoA reductase activity during hepatocarcinogenesis in rats. *Int. J. Biochem.*, **18**, 389–393.
44. Siperstein,M.D. (1984) Role of cholesterogenesis and isoprenoid synthesis in DNA replication and cell growth. *J. Lipid Res.*, **25**, 1462–1468.
45. Ontko,J.A., Perrin,L. and Horne,L.S. (1986) Isolation of hepatocellular lipid droplets: the separation of distinct subpopulations. *J. Lipid Res.*, **27**, 1097–1103.

Received on March 8, 1990; revised on June 11, 1990; accepted on June 18, 1990